Mechanism of miR-590-3p carried by tumor-derived extracellular vesicles in promoting invasion and metastasis of ovarian cancer

Yunyun Zheng
Xi'an Jiaotong University Second Affiliated Hospital
Kang Zhu
Xi'an Jiaotong University Second Affiliated Hospital
Guihu Wang (wangguihu0331@163.com)
Xi'an Jiaotong University Second Affiliated Hospital https://orcid.org/0000-0002-9633-6814

Research

Keywords: Ovarian cancer, Extracellular vesicles, miR-590-3p, CPEB3, Tumor microenvironment, Proliferation, Metastasis

Posted Date: April 20th, 2021

DOI: https://doi.org/10.21203/rs.3.rs-435550/v1

Abstract

Background

Ovarian cancer (OC) remains a common gynecologic malignancy. Tumor-derived extracellular vesicles (EVs) contribute to pro-metastasis microenvironment by carrying microRNAs (miRs). This study investigated the mechanism of miR-590-3p carried by OC cell-derived EVs in OC metastasis.

Methods

miR-590-3p expression in OC tissues and cells was measured. EVs were extracted from healthy serum and the serum of patients with OC or metastatic OC. EVs were extracted from OC cells and normal OC epithelial cells *in vitro*. miR-590-3p expression in EVs was tested. The effect of EVs-miR-590-3p on the proliferation, migration and invasion of OC cells was measured. The target of miR-590-3p was predicted and verified. The effect of miR-590-3p targeting CPEB3 on OC cells was confirmed by functional rescue assays. Xenograft tumor experiment was performed to verify the mechanism of EVs-miR-590-3p in the tumorigenesis and metastasis of OC.

Results

miR-590-3p expression was enhanced in OC, and correlated with OC metastasis. miR-590-3p was elevated in OC cell-derived EVs and could be transferred to other OC cells by EVs. OC cell-derived EVs facilitated proliferation, invasion and migration of OC cells by transferring miR-590-3p. miR-590-3p targeted CPEB3. Overexpressing CPEB3 repressed the promoting effect of EVs-miR-590-3p on OC cells. *In vivo* experiment confirmed that EVs-miR-590-3p facilitated tumorigenesis and metastasis of OC cells by targeting CPEB3.

Conclusion

OC cell-derived EVs facilitated progression and metastasis of OC via the miR-590-3p/CPEB3 axis.

Introduction

Ovarian cancer (OC) constitutes one of lethal gynaecological malignancy that affects female reproductive tract [1]. From the perspective of pathogenesis, OC encompasses histologically and genetically range of tumors, mainly originating from epithelial surface, stromal and germ cells [2]. The traditional therapeutic regimen for OC patients is mainly confined to tumor debulking surgery and subsequent chemotherapy [3]. Nevertheless, the bulk of OC patients fails to be diagnosed until dramatic symptoms occur, such as pelvic pain, abdominal distension and swelling or loss of appetite [4]. Owing to the lack of early detection, chemotherapy resistance, high recurrence and metastasis, and complicated

tumor microenvironment (TME), the OC patients have showed little improvement in unfavorable outcome in the past decades [5]. Hence, further clarifying the underlying mechanism of OC metastasis and determining novel therapeutic targets are urgent issues to be solved for the clinical management.

Extracellular vesicles (EVs), bioactive molecular shuttles packaged by proteins, lipids and nucleic acids, modulate TME by interacting with adjacent cells [6]. Tumor-derived EVs function as crucial mediators of intercellular communication between tumor cells and normal stromal cells in the local and distant TME, thereby facilitating tumor metastasis and invasion [7]. EVs participate in variant pathophysiological processes, including coagulation, vascular leakage and stromal receptor cell reprogramming to ensure the formation of pre-metastatic niche and subsequent metastasis [8]. EVs can be detected in ascites and blood of OC patients, making them the immense potential in minimally invasive diagnosis, drug selection, target treatment and prognostic evaluation involved in OC [9]. The tumorigenic effect of EVs has been characterized *in vivo* with the assistance of emerging technologies, which contributes to fully unveiling the clinical significance of these pro-metastatic factors in OC [7]. Understanding the progression and metastasis of OC from the perspective of EVs mechanism is essential for development of novel strategies for early diagnosis and therapies.

It is well established that tumor-derived EVs contribute to facilitating tumor progression and metastasis via their capacity of carrying multiple molecules, including microRNAs (miRs) [10]. miR has about 22 nucleotides in size, which functions as antisense RNA to downregulate the expression of target genes at post-transcription level [11]. Intriguingly, aberrant miR expression has been commonly accepted as a promising biomarker for the diagnosis and treatment of OC [12]. Emerging evidences have revealed that miR-590-3p expression is elevated in the serum of OC patients and contributes to OC progression [13, 14]. However, whether OC cell-derived EVs can affect the progression and metastasis of OC by carrying miR-590-3p in TME is unclear yet. This study herein investigated the effect of miR-590-3p carried by EVs on the invasion and metastasis of OC, which shall confer novel insights for the management of OC.

Materials And Methods

Patient sample

OC tissues and adjacent tissues were collected from 64 OC patients in Xi'an Jiaotong University Second Affiliated Hospital from January 2015 to January 2017. The patients were all female, aged 35–62 years, with an average age of 48.13 ± 5.98 years. The pathological diagnosis was based on the histology or biopsy of tumor specimens and examined by experienced pathologists. OC tissues and adjacent tissues were stored in liquid nitrogen. Since 2015, serum samples of 21 patients with non-metastatic OC, 43 patients with metastatic OC and 20 healthy controls were extracted.

Cell culture

Ovarian epithelial cells (IOSE 80) were purchased from BeNa Culture Collection (Suzhou, Jiangsu, China). OC cells [ES-2 (ATCC® CRL-1978), SKOV3 (ATCC® HTB-77) and Caov3 (ATCC® HTB-75)] and 293T cell

line (ATCC® CRL-1573) were obtained from ATCC (Manassas, Virginia, USA). All cell lines received detection of Mycoplasma and STR. IOSE 80 cells were cultured in MCDB105/Medium199 complete medium; OC cells were incubated in RPMI 1640 medium containing 10% fetal bovine serum (FBS), 100 IU/mL penicillin and 100 μg/mL streptomycin; 293T cells were cultured in Dulbecco's modified Eagle's medium (DMEM) with high glucose at 37℃ with 5% CO_2. After detached with 0.01% trypsin every 2–3 days, the cells were passaged routinely.

Isolation of EVs

For the treatment of cell supernatant, FBS (30067334, Thermo Fisher Scientific Inc., Waltham, MA, USA) was centrifuged at 4℃ and 1 × 10^6 g for 16 h (Beckman Coulter Avanti J-30I, Chaska, MN, USA) to deplete the effect of its own EVs. SKOV3 cells were cultured for 48–72 h. Then the medium was collected and the EVs were isolated by ultracentrifugation. For the treatment of serum samples, the blood was collected from blood vessels (anticoagulants must not be added to the collected serum samples), and left standing for 30 min. After standing at 4℃ for 3–4 h, blood clots could be seen. After the samples were centrifuged at 4℃ for 10 min at 1900 × g, light yellow serum could be seen. Then the supernatant was collected and centrifuged at 4℃ for 10 min at 3000 × g.

EVs were extracted by ultracentrifugation. The cell medium or treated serum was centrifuged at 300 g for 10 min, 2000 g for 15 min and 12000 g for 30 min, and then passed through the 22.0 μm filter. The supernatant was further centrifuged at 4℃ for 2 h at 1 × 10^6 g, washed in phosphate-buffered saline (PBS), and centrifuged for the second time under the same conditions. Thereafter, the precipitate was resuspended in 100 mL PBS and kept at -80℃ for standby or immediate use [15].

Identification of EVs

For the Nanoparticle tracking analysis (NTA) [15], each sample was tested three times (30 s/time). After the video recording was completed, the brightness was adjusted to the appropriate value, and the resolution threshold was less than 5/screen from the screen to the blue dot (false positive). The trajectory of each EVs in the screen was analyzed using the software. According to the principle of Brownian motion, the diameter and concentration of EVs were automatically converted. The original concentration was converted according to the dilution ratio.

For the observation under transmission electron microscope (TEM) [16], 20 μL ultracentrifuged fresh EVs samples were loaded into a carbon-coated copper electron microscope grid for 2 min and negatively stained with phosphotungstic acid solution (12501-23-4, Sigma-Aldrich, Merck KGaA, Darmstadt, Germany) for 5 min. The grid was washed with PBS 3 times to remove the excess phosphotungstic acid solution, and then kept semi-dried in filter paper. The image was observed under TEM (H7650, Hitachi, Tokyo, Japan) at 80kV.

The expressions of EVs specific surface markers Alix (rabbit-anti, ab76608, Abcam, Cambridge, MA, USA), CD9 (rabbit-anti, ab236630, 1:1000, Abcam), CD81 (rabbit-anti, ab109201, 1:1000, Abcam) and Calnexin (rabbit-anti, ab92573, 1:10000, Abcam) were detected.

Cell uptake of EVs

The purified EVs were labeled with green fluorescent PKH-67 (Sigma-Aldrich). EVs were resuspended in 1 mL Diluent C solution, and 4 μL PKH67 ethanol dye solution was added into 1 mL Diluent C to prepare into 4×10^{-6} M dye solution. Then, 1 mL EVs suspension was mixed with PKH-67 for 5 min, and the staining was terminated by incubation with 2 mL 1% EVs-free FBS for 1 min. The labeled EVs were centrifuged at 100000 × g for 2 h. The samples were collected and enriched in the sucrose at the density of 1.13–1.19 g/mL, and then the labeled EVs were collected [17]. The PKH-67-labeled EVs were incubated with OC cells at 37℃ for 12 h. The cells were fixed with 4% paraformaldehyde, rinsed with PBS, and stained with DAPI (D9542, Sigma-Aldrich).

For the EVs experiment of receptor OC cells (ES-2 and Caov3) uptaking cy3-miR-590-3p carried by SKOV3 cells, SKOV3 cells were delivered with cy3-miR-590-3p (GenePharma, Shanghai, China) in serum-free medium using Lipo3000 kit (L3000001, Invitrogen Inc., Carlsbad, CA, USA). After 6 h, the cells were placed in 10% serum medium free of EVs for 48 h-incubation. Afterwards, the supernatant was collected. EVs were isolated in line with the above-mentioned ultracentrifugation steps, and resuspended in PBS and added into OC cells. Likewise, the cells were fixed with 4% paraformaldehyde and rinsed with PBS. The cytoskeleton was labeled with Phalloidin-iFluor 488 reagent (1:1000, ab176753, Abcam) for 30 min, and the nuclei were stained with DAPI (D9542, Sigma-Aldrich). The uptake of EVs and EVs-miR-590-3p in OC cells was observed under fluorescence microscope (ECLIPSE E800, Nikon, Tokyo, Japan).

Binding of miR-590-3p to EVs

RNase experiment was performed to confirm whether miR was bound to EV surface or packaged in EVs. Briefly, EVs were resuspended with PBS and cultured with 20 μg/μL RNAse (Purelink RNase A, Life Technologies, Gaithersburg, MD, USA) at 37℃ for 20 min. The integrity of vesicle membrane was disrupted by Triton X-100 treatment, using radio-immunoprecipitation assay (RIPA) buffer for 20 min followed by the above RNase treatment. After RNase A incubation, the reaction was inhibited by lysis buffer and RNA was isolated.

Cell transfection

The lentiviral vectors encoding miR-590-3p or NC and overexpression of CPEB3 or CPEB3 NC were designed and produced by Genechem (Shanghai, China). The SKOV3 cells were infected with lentivirus at 20 times multiplicity of infection and then selected with 1 μg/mL puromycin for 3 days.

miR-590-3p mimic, miR-590-3p mimic-NC, miR-590-3p inhibitor, inhibitor-NC were produced by Genepharma (Shanghai, China). ES-2 and CAOV3 cells in logarithmic growth phase were seeded into 6-well plates (1×10^5 cells/well). The cells reached 75% confluence after 24 h of conventional culture. The cells were transfected using Lipofectamine 2000. Briefly, 250 μL serum-free Opti-MEM (51985042, GIBCO, Grand Island, NY, USA) was used to dilute 25 pmol of mimic or inhibitor and 10 μL Lipofectamin 2000, respectively. After standing for 5 min, the two liquids were evenly mixed together. After standing for 20

min, the mixture was added into the cell culture well. The transfected cells underwent 48 h-culture at 37℃ with 5% CO_2 for subsequent experiments.

Cell counting kit-8 (CCK-8) assay

The cell viability was measured using CCK-8 assay kit (Dojindo, Kyushu Island, Japan). The treated cells were seeded into 96-well plate (5×10^3 cells/well). On days 1st, 2rd, 3nd, 4th and 5th day, 10 μL CCK8 solution and 100 μL fresh medium were supplemented into each well and incubated at 37℃ for 1 h. The absorbance at 450 nm was measured by microplate reader (Bio-Rad 680, Bio-Rad, Hercules, CA, USA). The cell proliferation activity was expressed by subtracting the absorbance of the blank well from the absorbance of the experimental well.

Transwell assay

The cell migration and invasion were measured using Transwell assay. The apical chamber of the bottom membrane was coated with Matrigel (BD Bioscience, San Jose, CA, USA) (The matrigel was polymerized into gel at 37℃ for 30min, and the substrate membrane was hydrated before use) to conduct invasion assay. The migration assay was conducted without coating Matrigel. The cells were cultured in serum-free medium for 12 h, harvested and resuspended in serum-free medium (1×10^5 cells/mL). The basolateral chamber was added with the medium containing 10% FBS. Transwell chamber was supplemented with 100 μL cell suspension and subjected to 24 h-incubation at 37℃. The cells were fixed with 100% methanol and stained with 1% toluidine blue (Sigma-Aldrich). Five visual fields were selected, and the stained cells were observed under the inverted optical microscope (Axio Observer3, CarlZeiss, Germany).

Reverse transcription quantitative polymerase chain reaction (RT-qPCR)

Total RNA was extracted from cells using Trizol reagent (Invitrogen), and 1 μg total RNA was reverse transcribed into cDNA using Revert Aid first-strand cDNA synthesis kit (Fermentas, Life Sciences, Canada). Then, RT-qPCR analysis was performed using SYBR Premix ExTaq™ II in an ABI PRISM® 7900HT system (Takara, Kyoto, Japan). For miR analysis: EVs-miR was isolated using SeraMir EVssome RNA purification kit (System Biosciences, Mountain View, CA, USA). miR was extracted from cells using PureLink™miRNA extraction kit and synthetized into cDNA using TaqMan microRNA assay kit (Applied Biosystems, Foster City, CA, USA). The universal reverse primers provided by FastStart Universal SYBR Green Master Mix (Roche, Mannheim GmbH, Penzberg, Germany) and TaqMan microRNA assay kit were used for RT-qPCR. GAPDH and U6 acted as the internal reference. In addition, miR level in culture media, serum and EVs was normalized to cel-miR-39 with an exogenous reference. The relative expression of genes was calculated by $2^{-\triangle\triangle CT}$ method. The primers are shown in Table 1. Each well had 3 duplicated wells.

Table 1
Primer sequence for RT-qPCR

Gene	Primer sequence
Hsa-miR-590-3p	F: 5’- GCGTAATTTTATGTATAAGC – 3’
Cel-miR-39	F: 5’-GGTCACCGGGTGTAAATCAGCTTG – 3’
Human U6 snRNA	F: 5’-CTCGCTTCGGCAGCACA-3’
Human CPEB3	F: 5’- GAAAGGTAAACACTACCCTCCCA – 3’
	R: 5’- CCAGGAAGGCATTGTTAAGTGC – 3’
Human GAPDH	F: 5’- GGTGAAGGTCGGTGTGAACGGATTTGG – 3’
	R: 5’- TGTGCCGTTGAATTTGCCGTGAGTGG – 3’

Western blotting

The tissues and cells were lysed in enhanced RIPA lysate containing protease inhibitor (Boster Biological Technology Co., Ltd, Wuhan, Hubei, China). Then the protein concentration was tested using bicinchoninic acid (BCA) assay kit (Boster Biological Technology). The protein was separated by 10% SDS-PAGE, and then transferred to PVDF membranes (Merck Millipore, Billerica, MA, USA). The membranes were blocked with 5% skim milk for 2 h to block the nonspecific binding and cultured with the primary antibodies overnight at 4℃. Following rinsing with tris-buffered saline-tween (TBST) buffer three times, the membranes were incubated with horseradish peroxidase labeled secondary antibody at 37℃ for 1 h. Following TBST washes, the bands were developed and visualized using enhanced chemiluminesence reagent (Thermo Fisher). ChemiDoc XRS Plus luminescent image analyzer (Bio-Rad) was used fro imaging and photographing. The gray value of each band was quantified using Image J (National Institutes of Health Inc., Bethesda, MD, USA), with GAPDH as the internal reference. The antibodies were as follows: CPEB3 (rabbit-anti, ab10833, 1:1000, Abcam), GAPDH (ab8245, Abcam), rabbit secondary antibody (ab97051, 1:10000, Abcam).

Dual-luciferase reporter gene assay

CPEB3 3'UTR gene fragment was synthesized and introduced into pGL3-control (Promega, Madison, Wisconsin, USA) by endonuclease site. Complementary mutant (MUT) sites of seed sequence were designed on CPEB3 wild type (WT). The target fragment was inserted into pGL3-control vector by restriction endonuclease cleavage and T4 DNA ligase. The luciferase reporter plasmids WT and MUT were co-transfected into 293T cells with miR-590-3p mimic or miR-590-3p mimic-NC. After 48 h, the cells were lysed. The luciferase activity was detected on Luminometer TD-20/20 (E5311, Promeg) using dual-luciferase reporter assay system kit (Promega). Each experiment was repeated 3 times independently.

RNA immunoprecipitation (RIP)

RIP was conducted using EZ-Magna RIP RNA binding protein immunoprecipitation kit (Millipore). Briefly, the cells were collected and lysed in the frozen lysis buffer supplemented with protease inhibitor, RNase inhibitor and 1 mM phenylmethylsulfonyl fluoride. The lysis buffer was centrifuged at 14000 g for 15 min, and 50°L lysis buffer was stored as input. The protein extract (1 mg) was incubated with rabbit IgG (Proteintech, Rosemont, IL, USA) at 4℃ overnight and then treated with 30°L A/G protein magnetic beads at 4 ℃ for 4 h. Afterwards, the beads were washed 5 times, and the miR of co-immunoprecipitation was extracted using mirVana PARIS kit (Ambion, Austin, Texas, USA). The extracted miR was reverse transcribed and analyzed by real-time PCR. In addition, miR folding enrichment in immunoprecipitation samples was presented in the form of percentage input, with IgG as isotype control.

Animal experiment

Healthy BALB/c nude mice aged 4–6 weeks were purchased from Institute of Materia Medica, Chinese Academy of Medical Science (Beijing, China). Nude mice were raised in specific pathogen-free animal laboratory in different cages at 22–25℃, with humidity of 60%-65%, and maintained in light/dark cycle for 12 h. Water and food were provided ad libitum. All the mice were fed adaptively for 1 week, and the health condition was evaluated before experiment.

In the subcutaneous tumorigenesis experiment, SKOV3 cells had the highest tumorigenic rate. Briefly, 0.2 mL SKOV3 cell suspension (1×10^7 cells/mL) was injected subcutaneously into the right subcutaneous tissue of each mouse. Eight days after injection, the mice were assigned into five groups: control group (injected with PBS via tail vein), SKOV3-EVs group (injected with 10 μg SKOV3 cell-derived EVs via tail vein), EVs-miR-590-3p group (injected with 10 μg miR-590-3p lentivirus-infected SKOV3-EVs), EVs-miR-590-3p + oe-NC group (injected with 10 μg miR-590-3p lentivirus-infected SKOV3-EVs and oe-NC via tail vein), and EVs-miR-590-3p + oe-CPEB3 group (injected with 10 μg miR-590-3p lentivirus-infected SKOV3-EVs and oe-CPEB3 via tail vein), with 8 mice in each group. The injection site was observed regularly and the tumor volume was recorded. Vernier caliper was used to measure the long diameter and short diameter of each tumor mass as variables "A" and "B". The tumor volume was calculated as $V = AB^2/2$ [18]. After 5 weeks, the mice were euthanized with ≥ 100 mg/kg pentobarbital sodium. The tumor weight was measured, and the expressions of miR-590-3p and CPEB3 were detected.

Lung [19] and liver metastasis [20] models were established by tail vein injection or intrasplenic injection. For the tail vein lung metastasis experiment, 2×10^6 SKOV3 cells were injected into the nude mice via tail vein. For the intrasplenic metastasis experiment, nude mice were anesthetized with pentobarbital sodium (35–40 mg/kg), and the spleen was resected by laparotomy. Then 2×10^6 SKOV3 cells were injected into the spleen capsule of nude mice. After 14 days of SKOV3 cell injection, nude mice were grouped (8 mice in each group) and injected with 10 μg EVs or equivalent amount of oe-CPEB3 lentivirus twice a week for 1 month. Then the nude mice were euthanized and lung tissues and livers were taken for examination.

Hematoxylin and eosin (HE) staining

The lung and liver tissues of nude mice were fixed with formalin, embedded in paraffin and sliced (4 μm). The tissue sections were stained using HE staining kit (Beyotime Biotechnology Co., Ltd, Shanghai, China) to observed the metastasis of lung and liver. The stained sections were observed under the inverted optical microscope (Axio Observer3).

Statistical analysis

Data analysis was performed using the SPSS 21.0 (IBM Corp., Armonk, NY, USA). Data are described as mean ± standard deviation. Paired *t*-test was adopted to analyze the data between cancer tissues and adjacent tissues; unpaired *t*-test was used to analyzed the data between the other two groups. One-way ANOVA was adopted to analyze the data among multiple groups; two-way ANOVA was used to analyzed the cell viability at different times, and repeated measurement ANOVA was used to compare the tumor volume at different time points. Pearson correlation analysis was utilized to estimate the correlation between CPEB3 and miR-590-3p. The $p < 0.05$ meant a statistical difference.

Results

miR-590-3p was enhanced in the EVs of OC patients and correlated with OC metastasis

miR-590-3p is concerned with tumor metastasis [13, 14]. OC cells can secrete EVs to promote metastasis [21, 22]. To further explore whether OC cell-derived EVs promoted the occurrence and metastasis of OC by secreting miR-590-3p, we evaluated the relationship between miR-590-3p and OC. miR-590-3p expression in 64 pairs of OC tissues and adjacent non-cancer tissues was detected using RT-qPCR. As shown in Fig. 1A, miR-590-3p was upregulated in OC tissues compared with adjacent non-cancer tissues ($p < 0.05$). To investigate whether miR-590-3p expression was related to OC metastasis, we further analyzed miR-590-3p expression in 43 metastatic OC tissues and 21 non-metastatic OC tissues. miR-590-3p expression was elevated in metastatic OC tissues relative to that in non-metastatic OC tissues (Fig. 1B; $p < 0.05$). The correlation between miR-590-3p expression and clinical manifestations was further analyzed. As shown in Table 2, miR-590-3p expression was notably correlated with lymph node metastasis and clinical stage ($p < 0.05$), but not with age and differentiation ($p > 0.05$). The serum EVs were isolated and purified from healthy donors and OC patients. TEM and NTA showed that the secretion of serum EVs in OC patients was notably higher than that in healthy controls (Fig. 1C/D). Then, we analyzed miR-590-3p expression in different serum EVs (25 healthy controls, 21 non-metastatic OC patients and 43 metastatic OC patients). As shown in Fig. 1E, miR-590-3p expression in serum EVs of OC patients was higher than that in healthy controls. More importantly, miR-590-3p expression in serum EVs of metastatic OC patients was notably higher than that in non-metastatic OC patients ($p < 0.05$). Briefly, miR-590-3p was elevated in OC and concerned with OC metastasis.

Table 2
Correlation between miR-590-3p expression and clinical features (N = 64)

	miR-590-3p expression		
Clinical pathology factors	N	Mean ± SD	*p* value
Age (year)			
> 60	18	1.76 ± 0.28	0.8769
≤ 60	46	1.75 ± 0.21	
Lymph node metastasis			
Negative	22	1.78 ± 0.23	0.47989
Positive	42	1.74 ± 0.22	
Differentiation degree			
Poor	31	1.85 ± 0.24	0.0009
Moderate	17	1.70 ± 0.15	
Well	16	1.61 ± 0.18	
TNM classification			0.0001
I	20	1.61 ± 0.19	
II	17	1.73 ± 0.15	
III-A	27	1.87 ± 0.22	

EVs transferred miR-590-3p in tumor microenvironment

To further explore whether OC cells could secrete miR-590-3p through EVs to facilitate initiation and metastasis of OC, we detected miR-590-3p expression in OC cell lines (SKOV3, ES-2 and Caov3) and normal ovarian epithelial cells (IOSE 80). miR-590-3p expression in OC cells was notably higher than that in normal cells ($p < 0.05$; Fig. 2A), and SKOV3 cells showed the highest miR-590-3p expression, while ES-2 and Caov3 cells had the relatively lower miR-590-3p expression. Then the EVs were extracted from IOSE 80 cells and SKOV3 cells. EVs presented cup-shaped or spherical under TEM (Fig. 2B). NTA showed that the diameter of EVs was mainly distributed in the range of 40–120 nm (Fig. 2C). Western blotting revealed that EVs overexpressed Alix, CD81 and CD9, but not endoplasmic reticulum-associated protein Calnexin (Fig. 2D). These results indicated that EVs were successfully isolated. miR-590-3p expression in SKOV3-EVs was notably higher than that in IOSE 80-EVs ($p < 0.05$; Fig. 2E). Additionally, the protective effect of EVs on endogenous miR-590-3p was evaluated. miR-590-3p expression did not change after RNase treatment, while miR-590-3p expression was decreased notably after the combined treatment of RNase and Triton X-100, indicating that miR-590-3p was encapsulated in membrane rather than directly

release ($p < 0.05$; Fig. 2F). We further observed the internalization of SKOV3 cell-derived EVs by OC cells (ES-2 and Caov3). EVs were labeled with PKH67 and then cultured with ES-2 and Caov3 cells for 24 h. Obvious green fluorescence in the cells was observed under the fluorescence microscope, indicating that ES-2 and Caov3 could internalize SKOV3-EVs (Fig. 2G). Then the extracted EVs were co-incubated with ES-2 and Caov3 cells, and miR-590-3p expression was examined using RT-qPCR. Compared with IOSE 80-EVs treatment, SKOV3-EVs treatment notably enhanced miR-590-3p expression in ES-2 and Caov3 cells ($p < 0.05$; Fig. 2H). To further confirm that miR-590-3p was transferred by EVs, we transfected Cy3-labeled miR-590-3p mimic into SKOV3 cells, extracted EVs, and then co-cultured with ES-2 and Caov3 cells. The results revealed that Cy3-labeled red fluorescence could be observed in ES-2 and Caov3 cells (Fig. 2I). Taken together, miR-590-3p was highly expressed in OC cells and could be transferred to other OC cells by EVs.

OC cell-derived EVs facilitated proliferation, invasion and migration of OC cells by transferring miR-590-3p

To further determine the effect of EVs-miR-590-3p on OC cells, we infected SKOV3 cells with miR-590-3p lentivirus, extracted EVs and detected miR-590-3p expression in cells and EVs. The results revealed that miR-590-3p lentivirus notably increased miR-590-3p expression in SKOV3 cells and EVs ($p < 0.05$; Fig. 3A/B). ES-2 and Caov3 cells were further treated with IOSE 80-EVs, SKOV3-EVs, SKOV3-EVs-miR-NC and SKOV3-EVs-miR-590-3p. Compared with IOSE 80-EVs treatment, SKOV3-EVs treatment increased miR-590-3p expression; compared with SKOV3-EVs-miR-NC, SKOV3-EVs-miR-590-3p treatment also enhanced miR-590-3p expression in ES-2 and Caov3 cells ($p < 0.05$; Fig. 3C). Compared with IOSE 80-EVs treatment, SKOV3-EVs treatment facilitated proliferation, migration and invasion of ES-2 and Caov3 cells; compared with SKOV3-EVs-miR-NC treatment, SKOV3-EVs-miR-590-3p treatment showed a better promoting effect on malignant episodes of OC cells ($p < 0.05$; Fig. 3D-F). Taken together, OC cell-derived EVs facilitated proliferation, invasion and migration of OC cells by transferring miR-590-3p.

EVs-miR-590-3p targeted CPEB3 expression in OC cells

To determine the downstream mechanism of miR-590-3p carried by OC cell-derived EVs, we predicted the target genes of miR-590-3p through Targetscan, and found the binding site between miR-590-3p and CPEB3 3’UTR (Fig. 4A). CPEB3 participates in migration and invasion of OC [23, 24]. The luciferase activity of the miR-590-3p mimic + CPEB3 3'UTR-WT co-transfection group was notably lower than that of the mimic-NC + CPEB3 3'UTR-WT co-transfection group ($p < 0.05$); the luciferase activity of the miR-590-3p mimic + CPEB3 3'UTR-MUT co-transfection group was not obviously different from that of the mimic + CPEB3 3'UTR-MUT co-transfection group ($p > 0.05$) (Fig. 4B). CPEB3 expression in OC tissues was notably lower than that in adjacent tissues; CPEB3 expression in metastatic OC tissues was lowered relative to that in non-metastatic OC tissues ($p < 0.05$; Fig. 4C). CPEB3 expression was negatively correlated with miR-590-3p (Fig. 4D). CPEB3 expression in OC cells was notably lower than that in normal cells ($p < 0.05$; Fig. 4E).

miR may regulate its target by forming RNA-induced silencing complex (RISC). To further explore whether miR590-3p and CPEB3 were in RISC complex, we used anti-Ago2 antibody (a key component of RISC complex) to conduct RIP assay on ES-2 and Caov3 cell extracts. Compared with the control IgG immunoprecipitation, Ago2 microspheres enriched miR-590-3p and CPEB3 ($p < 0.05$; Fig. 4F). Compared with the mimic-NC group, the miR-590-3p mimic group showed reduced CPEB3 mRNA and protein; compared with the inhibitor-NC group, the miR-590-3p inhibitor group showed elevated CPEB3 mRNA and protein ($p < 0.05$; Fig. 4G/H). ES-2 and Caov3 cells treated with SKOV3-EVs had downregulated CPEB3 expression compared with those treated with IOSE 80-EVs ($p < 0.05$; Fig. 4I/J). These results suggested that OC cell-derived EVs targeted CPEB3 expression in OC cells by transferring miR-590-3p.

EVs-miR-590-3p facilitated OC cell proliferation and migration by repressing CPEB3

To determine the effect of EVs-miR-590-3p on OC cells by targeting CPEB3, we overexpressed CPEB3 in OC cells. The transfection efficiency of OE-CPEB3 was verified using RT-qPCR and Western blotting (Fig. 5A/B). Then ES-2 and Caov3 cells were co-treated with SKOV3-EVs and OE-CPEB3. Compared with EVs-miR-NC + OE-NC treatment, EVs-miR-NC + OE-CPEB3 treatment increased CPEB3 expression; compared with EVs-miR-590-3p + OE-NC treatment, EVs-miR-590-3p + OE-CPEB3 treatment promoted cpeb3 expression ($p < 0.05$; Fig. 5C). Compared with EVs-miR-NC + OE-NC treatment, EVs-miR-NC + OE-CPEB3 treatment repressed OC cell proliferation, migration and invasion; compared with EVs-miR-590-3p + OE-NC treatment, EVs-miR-590-3p + OE-CPEB3 treatment inhibited OC cell proliferation, migration and invasion ($p < 0.05$; Fig. 5E-G). Briefly speaking, EVs-miR-590-3p facilitated OC cell proliferation and migration, while CPEB3 overexpression reversed the promoting effect of EVs-miR-590-3p on OC cells.

EVs-miR-590-3p facilitated tumorigenesis and metastasis in vivo **by repressing CPEB3**

To further verify the role of EVs-miR-590-3p *in vivo*, we established a subcutaneous xenograft tumor model in nude mice to observe the effect of EVs-miR-590-3p on the tumorigenesis of OC cells. Eight days after injection of OC cells, SKOV3 cell-derived EVs or OE-CPEB3 plasmid were injected into mice via tail vein. Tumor growth curve and tumor weight in nude mice ($p < 0.05$; Fig. 6A/B) exhibited that SKOV3-EVs notably enhanced growth and weight of tumor cells; compared with SKOV3-EVs treatment, EVs-miR-590-3p treatment enhanced tumorigenesis and tumor weight; compared with EVs-miR-590-3p + oe-NC treatment, EVs-miR-590-3p + OE-CPEB3 treatment reduced tumorigenesis and tumor weight. Expressions of miR-590-3p and CPEB3 in tumor tissues were detected. Compared with the control mice, SKOV3-EVs treatment notably increased miR-590-3p expression; compared with SKOV3-EVs treatment, EVs-miR-590-3p treatment enhanced miR-590-3p expression and reduced CPEB3 expression; compared with EVs-miR-590-3p + oe-NC treatment, EVs-miR-590-3p + OE-CPEB3 treatment increased CPEB3 expression ($p < 0.05$; Fig. 6C/D). Compared with the control mice, SKOV3-EVs treatment notably increased lung and liver metastasis of tumor cells; compared with SKOV3-EVs treatment, EVs-miR-590-3p treatment enhanced lung and liver metastasis of tumor cells; compared with EVs-miR-590-3p + oe-NC treatment, EVs-miR-590-

3p + OE-CPEB3 treatment suppressed lung and liver metastasis of tumor cells ($p < 0.05$; Fig. 6E/F). In brief, EVs-miR-590-3p facilitated tumorigenesis and metastasis *in vivo* by repressing CPEB3.

Discussion

OC patients hardly exhibit obvious clinical manifestations at the early stage, and most cases have developed into metastatic OC at the time of diagnosis [25]. Tumor-derived EVs are accepted as pivotal mediators of tumor progression and metastasis [26]. Here we demonstrated the effect of OC cell-derived EVs on OC progression metastasis via transferring miR-590-3p (Fig. 7).

Tumor-derived EVs act as crucial regulators of intercellular communication, contributing to facilitating tumor progression and metastasis [8]. OC cell-derived EVs carrying miRs can work as biomarkers of OC diagnosis and prognosis [27]. Accumulating evidences have unveiled the critical role of miR-590-3p in tumor progression, either as an oncogene or tumor suppressor [28–30]. Notably, an RNA-seq research has identified the aberrant expression of miR-590-3p in epithelial OC [31]. To further determine whether OC cell-derived EVs promoted the occurrence and metastasis of OC by carrying miR-590-3p, we evaluated the relationship between miR-590-3p and OC. miR-590-3p expression was enhanced in OC, and importantly, miR-590-3p in metastatic OC tissues was higher than that in non-metastatic OC tissues. Then, the serum EVs were isolated and purified from healthy donors and OC patients. The secretion of serum EVs in OC patients was notably higher than that in healthy controls. miR-590-3p expression in serum EVs of metastatic OC patients was notably higher than that in non-metastatic OC patients. Consistently, emerging evidences have revealed that miR-590-3p is upregulated in the plasma of OC patients, which enhances OC growth and metastasis and increases the aggressiveness of OC [13, 14]. Taken together, miR-590-3p was highly expressed in OC and associated with OC metastasis.

Then we extracted EVs from IOSE 80 cells and SKOV3 cells. miR-590-3p expression in SKOV3-EVs was notably higher than that in IOSE 80-EVs. Further experiments confirmed that miR-590-3p could be transferred to other OC cells by EVs. To further determine the effect of EVs-miR-590-3p on OC cells, we infected SKOV3 cells with miR-590-3p lentivirus, and then extracted EVs. ES-2 and Caov3 cells were treated with IOSE 80-EVs, SKOV3-EVs, SKOV3-EVs-miR-NC and SKOV3-EVs-miR-590-3p. SKOV3-EVs facilitated proliferation, migration and invasion of ES-2 and Caov3 cells; SKOV3-EVs-miR-590-3p treatment showed a better promoting effect on OC cells. Collectively, OC cell-derived EVs facilitated malignant transformation of OC cells by transferring miR-590-3p.

Then, we shifted to determining the target of miR-590-3p in OC metastasis. CPEB is an RNA binding protein, which interacts with the cytoplasmic polyadenylation element or U-rich sequence in the 3'UTR of specific mRNA to activate or suppress translation [32]. CPEB has received increasing concerns due to its function of modulating gene expression associated with tumor malignant transformation [33]. Altered CPEB3 expression indicates its regulatory role in some genital cancers, including OC [24]. CPEB3 expression is reduced in OC tissues and cells, and targeting CPEB3 can accelerate migration and invasion of high-grade OC [23]. Consistently, we exhibited that CPEB3 expression was reduced in OC, and CPEB3 in

metastatic OC was lower than that in non-metastatic OC. miR cleaves highly complementary targets with the assistant of an Ago2-dependent slicer, a component of RISC [34]. We used anti-Ago2 antibody to conduct RIP assay on ES-2 and Caov3 cell extracts. The results revealed that Ago2 microspheres enriched miR-590-3p and CPEB3. ES-2 and Caov3 cells treated with SKOV3-EVs had downregulated CPEB3 expression compared with those treated with IOSE 80-EVs. In brief, OC cell-derived EVs targeted CPEB3 expression in OC cells by transferring miR-590-3p. ES-2 and Caov3 cells were co-treated with SKOV3-EVs and OE-CPEB3. The results implied that the malignant transformation of OC cells was repressed notably, indicating that CPEB3 overexpression abated the function of EVs-miR-590-3p in OC cells. *In vivo* experiments verified that EVs-miR-590-3p facilitated tumorigenesis and metastasis, and CPEB3 overexpression could alleviate this effect.

Conclusions

OC cell-derived EVs carried miR-590-3p into OC cells, thereby facilitating OC metastasis via targeting CPEB3. Whether the miR-590-3p/CPEB3 axis mediated by EVs can function as a therapeutic entry point for OC needs further exploration. In the future, we shall conduct more *in vivo* experiments to investigate the mechanism of miR-590-3p/CPEB3 axis in OC progression and metastasis in depth.

Declarations

Author contributions

Yunyun Zheng contributed to the conception, Kang Zhu completed the experiments. Yunyun Zheng and Kang Zhu drafted the manuscript, Guihu Wang critically revised the manuscript. All authors contributed to the article and approved the submitted version.

Funding

The authors did not receive support from any organization for the submitted work.

Availability of data and materials

All experimental datasets generated for this study are included in the article.

Ethics approval and consent to participate

This study got the approval of the Ethics Committee of Xi'an Jiaotong University Second Affiliated Hospital, following the Declaration of Helsinki. The informed consent was conferred by each eligible participant. The animals were treated on the basis of the standards of animal ethics.

Consent for publication

All the participants consent for publication.

Competing interests

The authors have no relevant financial or non-financial interests to disclose.

Author details

[1]National-Local Joint Engineering Research Center of Biodiagnostics and Biotherapy, Xi'an Jiaotong University Second Affiliated Hospital, Xi’an, Shaanxi, People’s Republic of China

[2]Department of Obstetrics and Gynecology, Xi'an Jiaotong University Second Affiliated Hospital, Xi’an, Shaanxi, People’s Republic of China

Acknowledgements

Thanks to everyone who has made contribution to this article.

References

1. Lisio MA, Fu L, Goyeneche A, Gao ZH, Telleria C. High-Grade Serous Ovarian Cancer: Basic Sciences, Clinical and Therapeutic Standpoints. Int J Mol Sci. 2019;20(4).
2. Karnezis AN, Cho KR, Gilks CB, Pearce CL, Huntsman DG. The disparate origins of ovarian cancers: pathogenesis and prevention strategies. Nat Rev Cancer. 2017;17(1):65-74.
3. Komiyama S, Katabuchi H, Mikami M, Nagase S, Okamoto A, Ito K, Morishige K, Suzuki N, Kaneuchi M, Yaegashi N, Udagawa Y, Yoshikawa H. Japan Society of Gynecologic Oncology guidelines 2015 for the treatment of ovarian cancer including primary peritoneal cancer and fallopian tube cancer. Int J Clin Oncol. 2016;21(3):435-446.
4. Elias KM, Fendler W, Stawiski K, Fiascone SJ, Vitonis AF, Berkowitz RS, Frendl G, Konstantinopoulos P, Crum CP, Kedzierska M, Cramer DW, Chowdhury D. Diagnostic potential for a serum miRNA neural network for detection of ovarian cancer. Elife. 2017;6.
5. Novak C, Horst E, Mehta G. Review: Mechanotransduction in ovarian cancer: Shearing into the unknown. APL Bioeng. 2018;2(3):031701.
6. Giusti I, Di Francesco M, D'Ascenzo S, Palmerini MG, Macchiarelli G, Carta G, Dolo V. Ovarian cancer-derived extracellular vesicles affect normal human fibroblast behavior. Cancer Biol Ther. 2018;19(8):722-734.
7. Feng W, Dean DC, Hornicek FJ, Shi H, Duan Z. Exosomes promote pre-metastatic niche formation in ovarian cancer. Mol Cancer. 2019;18(1):124.
8. Becker A, Thakur BK, Weiss JM, Kim HS, Peinado H, Lyden D. Extracellular Vesicles in Cancer: Cell-to-Cell Mediators of Metastasis. Cancer Cell. 2016;30(6):836-848.
9. Tang MK, Wong AS. Exosomes: Emerging biomarkers and targets for ovarian cancer. Cancer Lett. 2015;367(1):26-33.

10. Xu R, Rai A, Chen M, Suwakulsiri W, Greening DW, Simpson RJ. Extracellular vesicles in cancer - implications for future improvements in cancer care. Nat Rev Clin Oncol. 2018;15(10):617-638.
11. Ghafouri-Fard S, Shoorei H, Taheri M. miRNA profile in ovarian cancer. Exp Mol Pathol. 2020;113:104381.
12. Deb B, Uddin A, Chakraborty S. miRNAs and ovarian cancer: An overview. J Cell Physiol. 2018;233(5):3846-3854.
13. Salem M, Shan Y, Bernaudo S, Peng C. miR-590-3p Targets Cyclin G2 and FOXO3 to Promote Ovarian Cancer Cell Proliferation, Invasion, and Spheroid Formation. Int J Mol Sci. 2019;20(8).
14. Salem M, O'Brien JA, Bernaudo S, Shawer H, Ye G, Brkic J, Amleh A, Vanderhyden BC, Refky B, Yang BB, Krylov SN, Peng C. miR-590-3p Promotes Ovarian Cancer Growth and Metastasis via a Novel FOXA2-Versican Pathway. Cancer Res. 2018;78(15):4175-4190.
15. Yan W, Wu X, Zhou W, Fong MY, Cao M, Liu J, Liu X, Chen CH, Fadare O, Pizzo DP, Wu J, Liu L, Liu X, Chin AR, Ren X, Chen Y, Locasale JW, Wang SE. Cancer-cell-secreted exosomal miR-105 promotes tumour growth through the MYC-dependent metabolic reprogramming of stromal cells. Nat Cell Biol. 2018;20(5):597-609.
16. Hu M, Guo G, Huang Q, Cheng C, Xu R, Li A, Liu N, Liu S. The harsh microenvironment in infarcted heart accelerates transplanted bone marrow mesenchymal stem cells injury: the role of injured cardiomyocytes-derived exosomes. Cell Death Dis. 2018;9(3):357.
17. Puzar Dominkus P, Stenovec M, Sitar S, Lasic E, Zorec R, Plemenitas A, Zagar E, Kreft M, Lenassi M. PKH26 labeling of extracellular vesicles: Characterization and cellular internalization of contaminating PKH26 nanoparticles. Biochim Biophys Acta Biomembr. 2018;1860(6):1350-1361.
18. Li J, Xu J, Li L, Ianni A, Kumari P, Liu S, Sun P, Braun T, Tan X, Xiang R, Yue S. MGAT3-mediated glycosylation of tetraspanin CD82 at asparagine 157 suppresses ovarian cancer metastasis by inhibiting the integrin signaling pathway. Theranostics. 2020;10(14):6467-6482.
19. Dou C, Xu Q, Liu J, Wang Y, Zhou Z, Yao W, Jiang K, Cheng J, Zhang C, Tu K. SHMT1 inhibits the metastasis of HCC by repressing NOX1-mediated ROS production. J Exp Clin Cancer Res. 2019;38(1):70.
20. Bartolome RA, Martin-Regalado A, Jaen M, Zannikou M, Zhang P, de Los Rios V, Balyasnikova IV, Casal JI. Protein Tyrosine Phosphatase-1B Inhibition Disrupts IL13Ralpha2-Promoted Invasion and Metastasis in Cancer Cells. Cancers (Basel). 2020;12(2).
21. Zhang X, Sheng Y, Li B, Wang Q, Liu X, Han J. Ovarian cancer derived PKR1 positive exosomes promote angiogenesis by promoting migration and tube formation in vitro. Cell Biochem Funct. 2021;39(2):308-316.
22. Zhang Q, Len TY, Zhang SX, Zhao QH, Yang LH. Exosomes transferring long non-coding RNA FAL1 to regulate ovarian cancer metastasis through the PTEN/AKT signaling pathway. Eur Rev Med Pharmacol Sci. 2020;24(1):43-54.
23. Liu F, Zhang G, Lv S, Wen X, Liu P. miRNA-301b-3p accelerates migration and invasion of high-grade ovarian serous tumor via targeting CPEB3/EGFR axis. J Cell Biochem. 2019;120(8):12618-12627.

24. Hansen CN, Ketabi Z, Rosenstierne MW, Palle C, Boesen HC, Norrild B. Expression of CPEB, GAPDH and U6snRNA in cervical and ovarian tissue during cancer development. APMIS. 2009;117(1):53-59.
25. Chen SN, Chang R, Lin LT, Chern CU, Tsai HW, Wen ZH, Li YH, Li CJ, Tsui KH. MicroRNA in Ovarian Cancer: Biology, Pathogenesis, and Therapeutic Opportunities. Int J Environ Res Public Health. 2019;16(9).
26. Yokoi A, Yoshioka Y, Yamamoto Y, Ishikawa M, Ikeda SI, Kato T, Kiyono T, Takeshita F, Kajiyama H, Kikkawa F, Ochiya T. Malignant extracellular vesicles carrying MMP1 mRNA facilitate peritoneal dissemination in ovarian cancer. Nat Commun. 2017;8:14470.
27. Chen J, Fei X, Wang J, Cai Z. Tumor-derived extracellular vesicles: Regulators of tumor microenvironment and the enlightenment in tumor therapy. Pharmacol Res. 2020;159:105041.
28. Zu C, Liu S, Cao W, Liu Z, Qiang H, Li Y, Cheng C, Ji L, Li J, Li J. MiR-590-3p suppresses epithelial-mesenchymal transition in intrahepatic cholangiocarcinoma by inhibiting SIP1 expression. Oncotarget. 2017;8(21):34698-34708.
29. Sun ZQ, Shi K, Zhou QB, Zeng XY, Liu J, Yang SX, Wang QS, Li Z, Wang GX, Song JM, Yuan WT, Wang HJ. MiR-590-3p promotes proliferation and metastasis of colorectal cancer via Hippo pathway. Oncotarget. 2017;8(35):58061-58071.
30. Abdolvahabi Z, Nourbakhsh M, Hosseinkhani S, Hesari Z, Alipour M, Jafarzadeh M, Ghorbanhosseini SS, Seiri P, Yousefi Z, Yarahmadi S, Golpour P. MicroRNA-590-3P suppresses cell survival and triggers breast cancer cell apoptosis via targeting sirtuin-1 and deacetylation of p53. J Cell Biochem. 2019;120(6):9356-9368.
31. Keller A, Backes C, Leidinger P, Kefer N, Boisguerin V, Barbacioru C, Vogel B, Matzas M, Huwer H, Katus HA, Stahler C, Meder B, Meese E. Next-generation sequencing identifies novel microRNAs in peripheral blood of lung cancer patients. Mol Biosyst. 2011;7(12):3187-3199.
32. Fernandez-Miranda G, Mendez R. The CPEB-family of proteins, translational control in senescence and cancer. Ageing Res Rev. 2012;11(4):460-472.
33. Fang Y, Zhong Q, Wang Y, Gu C, Liu S, Li A, Yan Q. CPEB3 functions as a tumor suppressor in colorectal cancer via JAK/STAT signaling. Aging (Albany NY). 2020;12(21):21404-21422.
34. O'Brien J, Hayder H, Zayed Y, Peng C. Overview of MicroRNA Biogenesis, Mechanisms of Actions, and Circulation. Front Endocrinol (Lausanne). 2018;9:402.

Figures

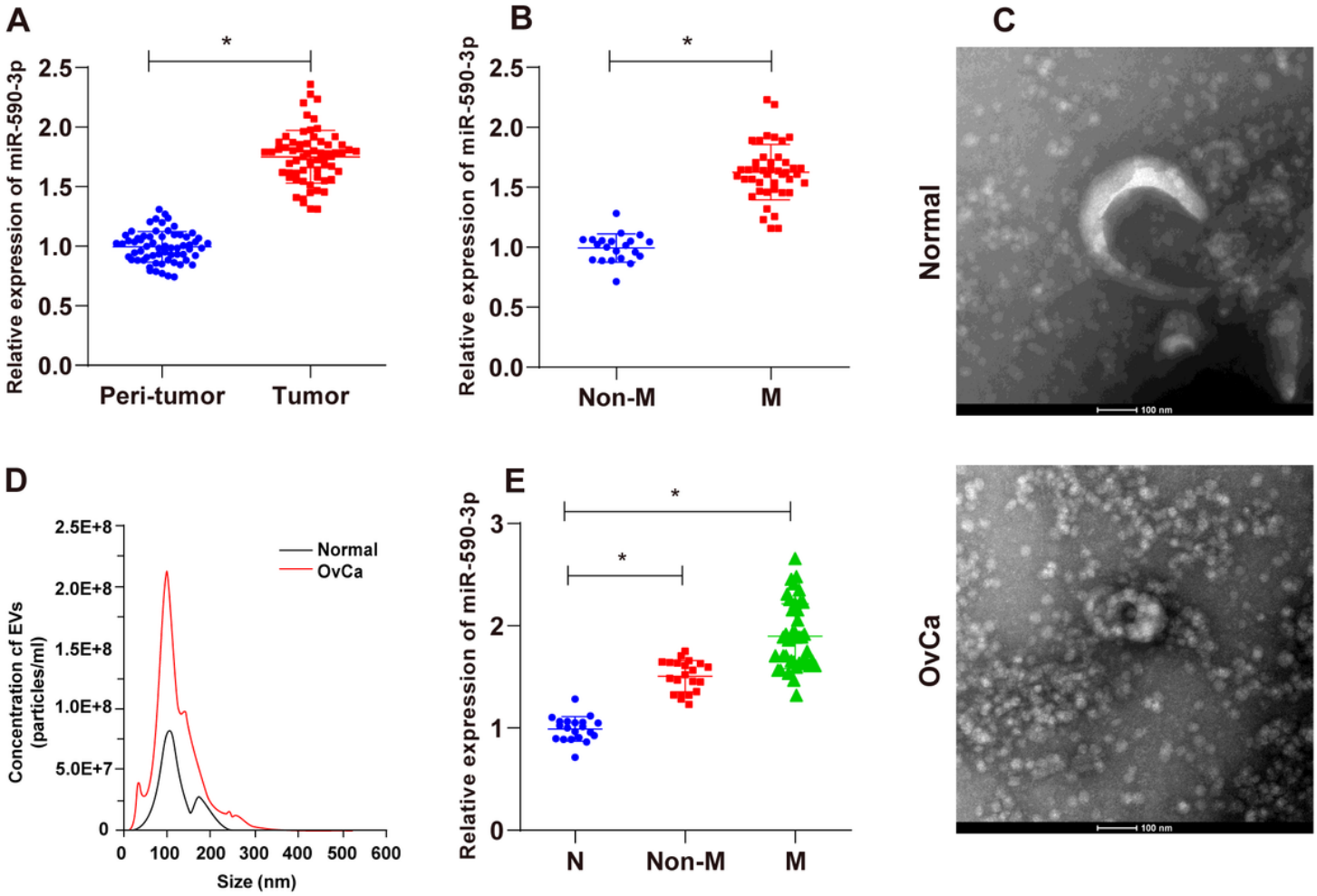

Figure 1

miR-590-3p was highly expressed in EVs derived from OC patients and EVs mediated the transferring of miR-590-3p. A: RT-qPCR demonstrated that miR-590-3p expression in OC tissues was higher than that in adjacent tissues (N = 64). B: RT-qPCR showed that miR-590-3p expression in metastatic OC tissues was higher than that in non-metastatic OC tissues. C: The morphology of EVs in serum of healthy donors and OC patients was observed under TEM, scale bar = 200 nm. D: The size distribution and concentration of EVs in serum of healthy donors and OC patients were measured by NTA. E: miR-590-3p expression in serum of healthy donors and OC patients. N: Normal controls, N= 20; Non-M: OC patients without metastasis; N = 21; M: OC patients with metastasis, N = 43. Data are presented as mean ± standard deviation. Paired t-test was adopted to analyze the data between cancer tissues and adjacent tissues; unpaired t-test was used to analyzed the data between the other two groups, and one-way ANOVA was used to analyze the data among multiple groups.

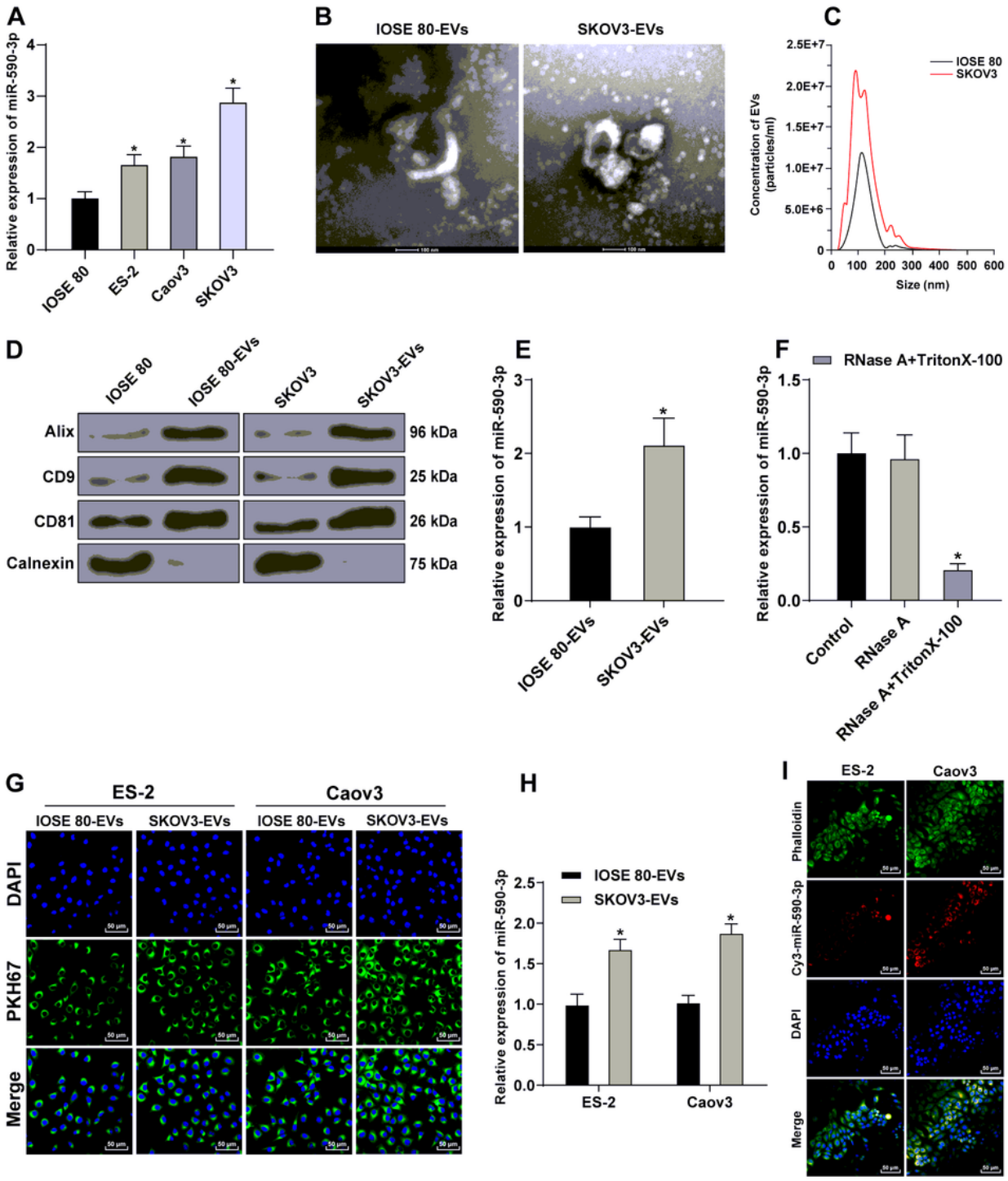

Figure 2

EVs transferred miR-590-3p in tumor microenvironment. A: miR-590-3p expression in OC cell lines (SKOV3, ES-2 and Caov3) and normal ovarian epithelial cells (IOSE 80) was detected using RT-qPCR. B: The morphology of EVs was observed under TEM, bar = 100 nm. C: The size distribution of EVs was measured by NTA. D: The specific surface marker proteins of EVs were tested using Western blotting. E: SKOV3-EVs were extracted and miR-590-3p expression in EVs was detected using RT-qPCR. F: EVs were

co-treated with RNase and Triton X-100, and miR-590-3p expression in EVs was detected using RT-qPCR. G: EVs were labeled with PKH67 and cultured with ES-2 and Caov3 cells for 24 h; the internalization of EVs by OC cells was observed under the fluorescence microscope; H: SKOV3-EVs were extracted and cultured with ES-2 and Caov3 cells; miR-590-3p expression in cells was detected using RT-qPCR. I: The cy3-miR-590-3p-labeled SKOV3-EVs into ES-2 and CAOV3 cells was observed by laser confocal; EVs labeled with cy3-miR-590-3p was red, and the nuclei was stained blue by DAPI; ES-2 or Caov3 cells were stained green by phalloidin scale bar = 20 μm. Data are presented as mean ± standard deviation. The experiment was repeated 3 times independently. Unpaired t-test was adopted to analyzed the data between two groups, and one-way ANOVA was used to analyze the data among multiple groups. * vs. the IOSE 80 group, $p < 0.05$; # vs. the SKOV3 group, $p < 0.05$.

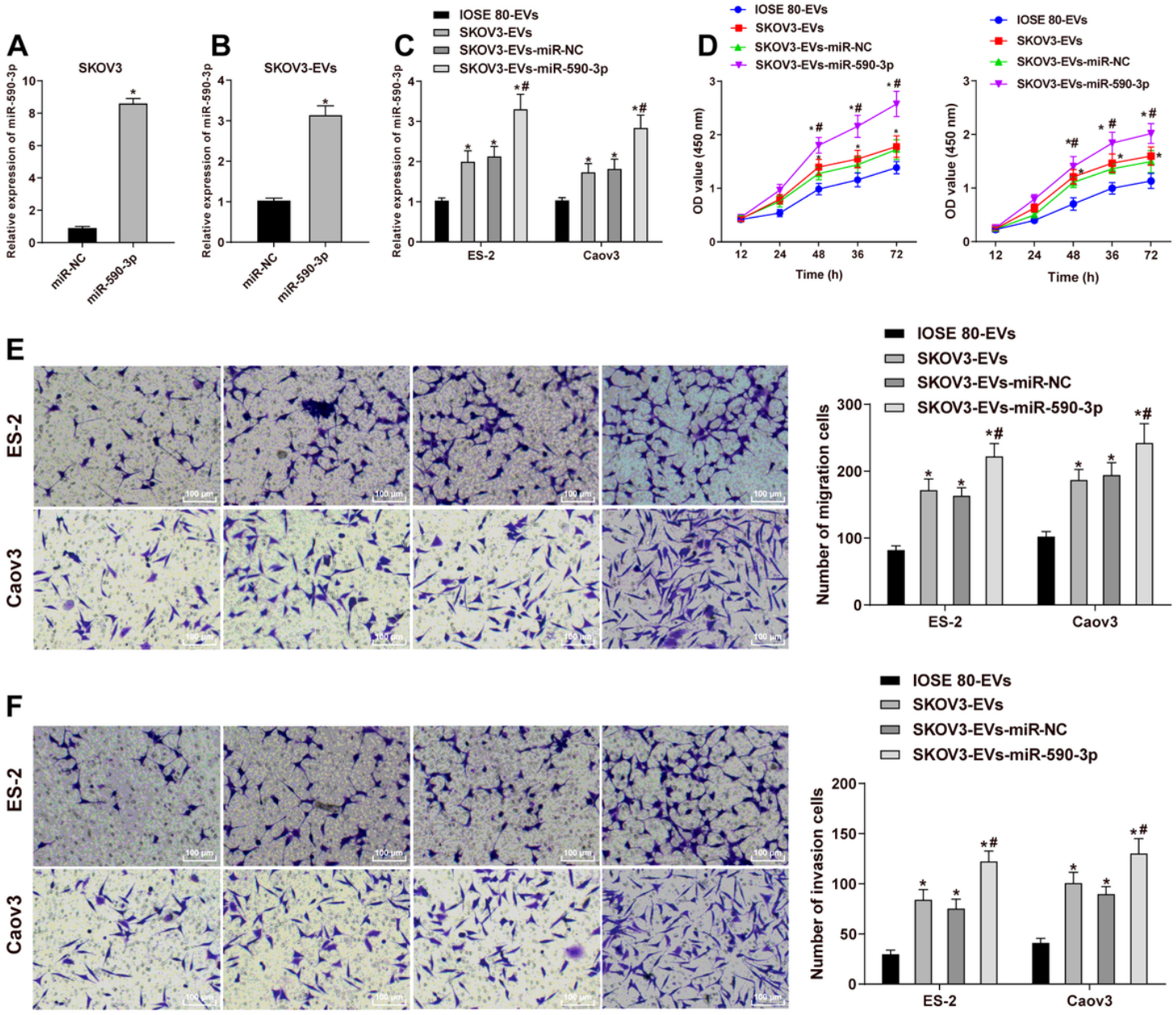

Figure 3

OC cell-derived EVs facilitated proliferation, invasion and migration of OC cells by transferring miR-590-3p. A: SKOV3 cells were infected with miR-590-3p lentivirus, and miR-590-3p expression in SKOV3 cells was detected using RT-qPCR. B: SKOV3 cells were infected with miR-590-3p lentivirus and EVs were extracted; miR-590-3p expression in EVs was detected using RT-qPCR. C: ES-2 and Caov3 cells were further treated with IOSE 80-EVs, SKOV3-EVs, SKOV3-EVs-miR-NC and SKOV3-EVs-miR-590-3p, and miR-590-3p expression in cells was detected using RT-qPCR. D: The cell proliferation was measured using CCK-8 assay. E/F: The cell migration and invasion were measured using Transwell assay, scale bar = 50 μm. Data are presented as mean ± standard deviation. The experiment was repeated 3 times independently. Unpaired t-test was adopted to analyzed the data between two groups; one-way ANOVA was used to analyze the data among multiple groups, and two-way ANOVA was used to analyzed the data between two groups at different time points. Figure A/B, * vs. the miR-NC group, $p < 0.05$; Figure C/D/E/F, * vs. the IOSE 80-EVs group, $p < 0.05$, # vs. the SKOV3-EVs-miR-NC group, $p < 0.05$.

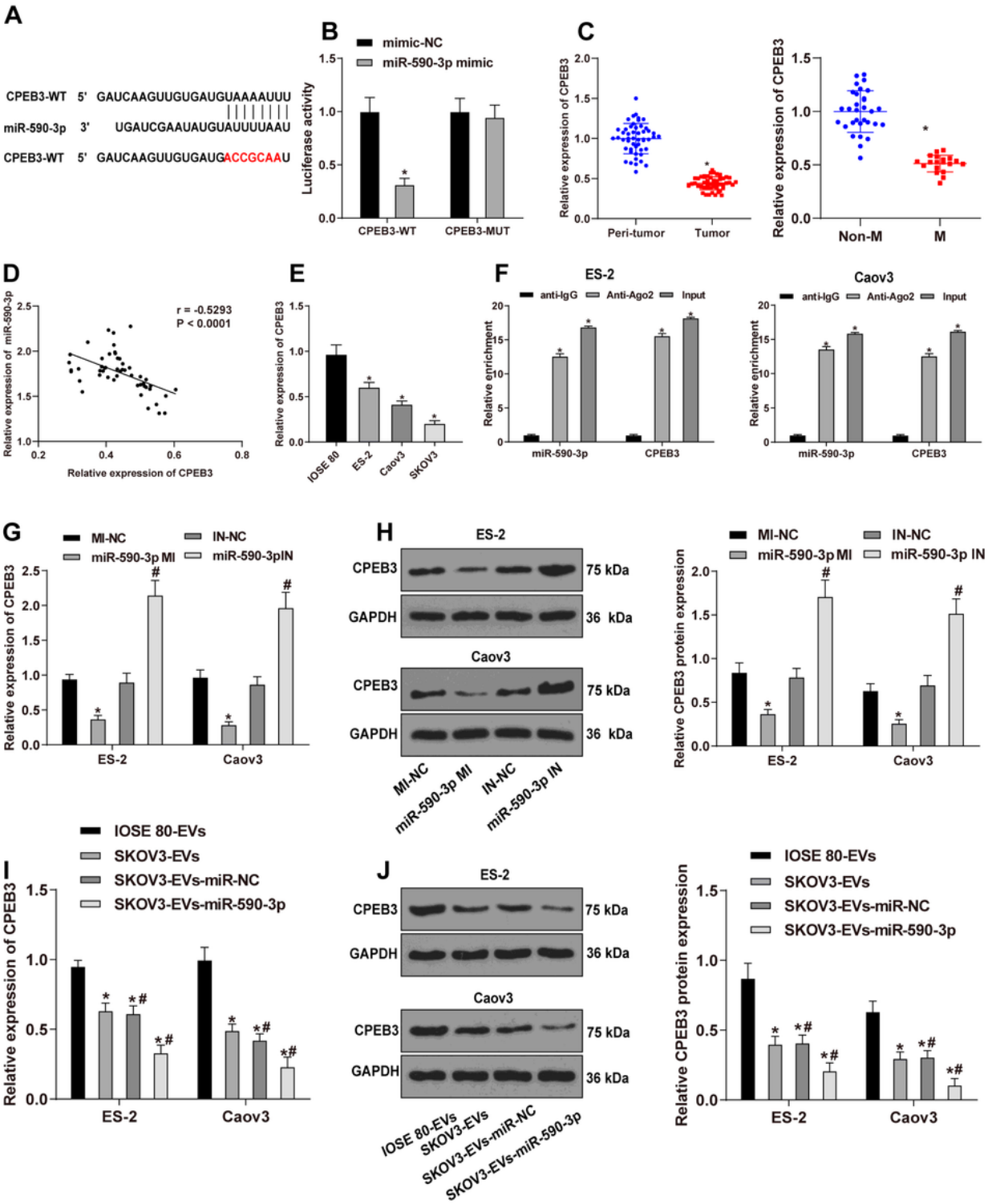

Figure 4

EVs-miR-590-3p targeted CPEB3 expression in OC cells. A: The specific binding sites and targeted mutation sites of CPEB3 and miR-590-3p were predicted through Targetscan. B: Luciferase activity was detected using dual-luciferase reporter gene assay, * vs. the mimic-NC group, $p < 0.05$. C: CPEB3 expression in OC tissues and adjacent tissues (N = 64), metastatic OC tissues and non-metastatic OC tissues was detected using RT-qPCR, * vs. the Peri-Tumor group or Non-M group, $p < 0.05$. D: The

correlation between CPEB3 and miR-590-3p expression was analyzed by Pearson. E: CPEB3 expression in OC cell lines and normal ovarian epithelial cells was detected using RT-qPCR. F: Ago2 antibody was extracted from ES-2 and Caov3 cells for RIP; miR-590-3p and CPEB3 mRNA expression were detected using RT-qPCR. G: CPEB3 expression in ES-2 and Caov3 cells transfected with miR-590-3p mimic (MI) or inhibitor (IN) was detected using RT-qPCR, * vs. the mimic (MI)-NC group, $p < 0.05$, # vs. the inhibitor (IN)-NC group, $p < 0.05$. H: CPEB3 protein level in ES-2 and Caov3 cells transfected with miR-590-3p mimic (MI) or inhibitor (IN) was detected using Western blotting, * vs. the miR-NC group, $p < 0.05$, # vs. the inhibitor-NC group, $p < 0.05$. I/J: CPEB3 expression in EVs-treated ES-2 and Caov3 cells was detected using RT-qPCR and Western blotting, * vs. the IOSE 80-EVs group, $p < 0.05$. Data are presented as mean ± standard deviation. The experiment was repeated 3 times independently. Paired t-test was adopted to analyzed the data between cancer tissues and adjacent tissues; unpaired t-test was used to analyzed the data between the other two groups, and one-way ANOVA was used to analyze the data among multiple groups.

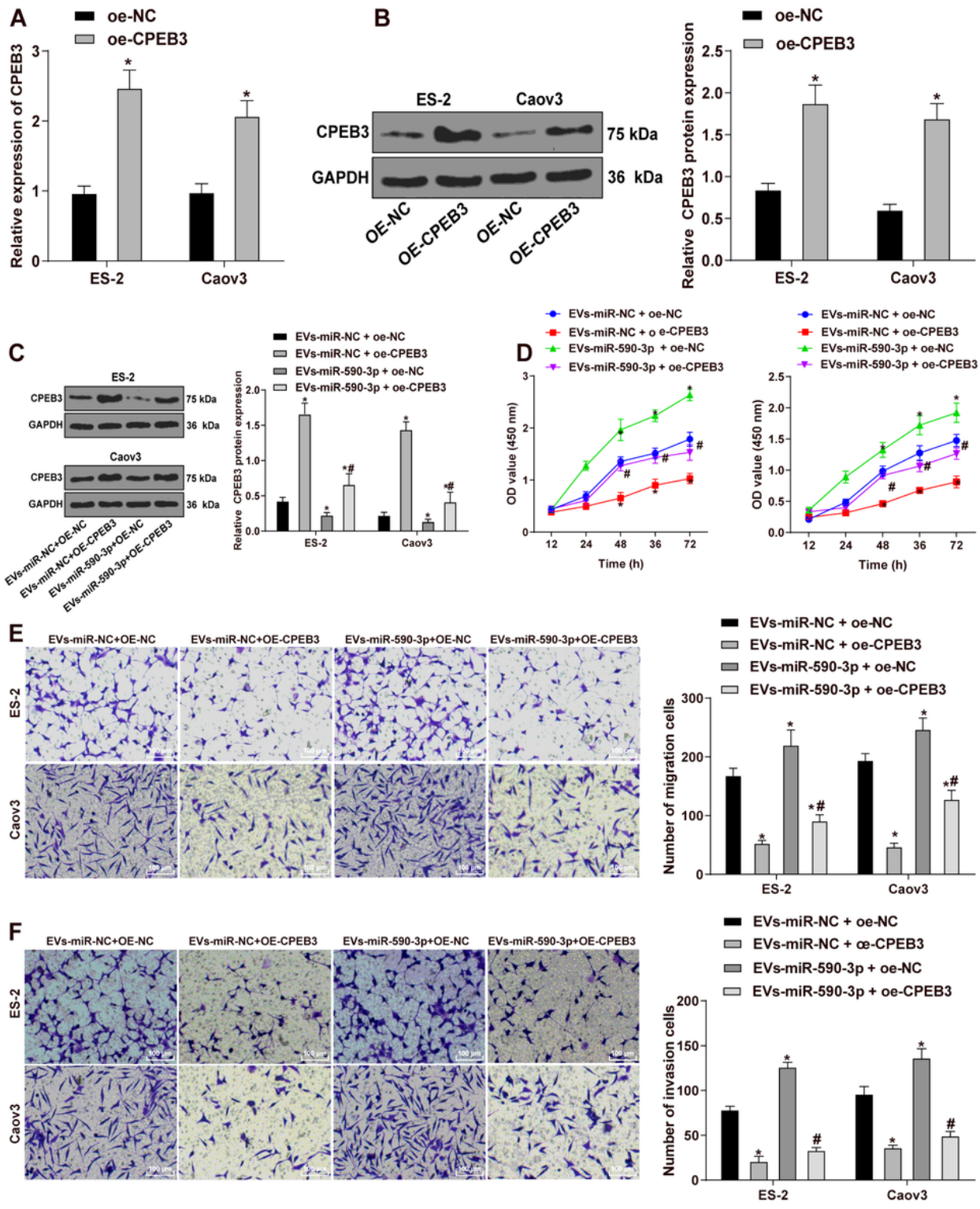

Figure 5

EVs-miR-590-3p facilitated OC cell proliferation and migration by repressing CPEB3. A/B: Transfection efficiency of OE-CPEB3 in ES-2 and Caov3 cells was confirmed using RT-qPCR and Western blotting. C: ES-2 and Caov3 were treated with SKOV3-EVs and OE-CPEB3, and CPEB3 expression was detected using Western blotting. D: The cell proliferation was measured using CCK-8 assay. E/F: The cell migration and invasion were measured using Transwell assay, scale bar = 50 μm. Data are presented as mean ±

standard deviation. The experiment was repeated 3 times independently. Unpaired t-test was adopted to analyzed the data between two groups; one-way ANOVA was used to analyze the data among multiple groups, and two-way ANOVA was used to analyzed the data between two groups at different time points. Figure A/B, * vs. the OE-NC group, $p < 0.05$; Figure C/D/E/F, * vs. the EVs-miR-NC + OE-NC group, $p < 0.05$, # vs. the EVs-miR-590-3p + OE-NC group, $p < 0.05$.

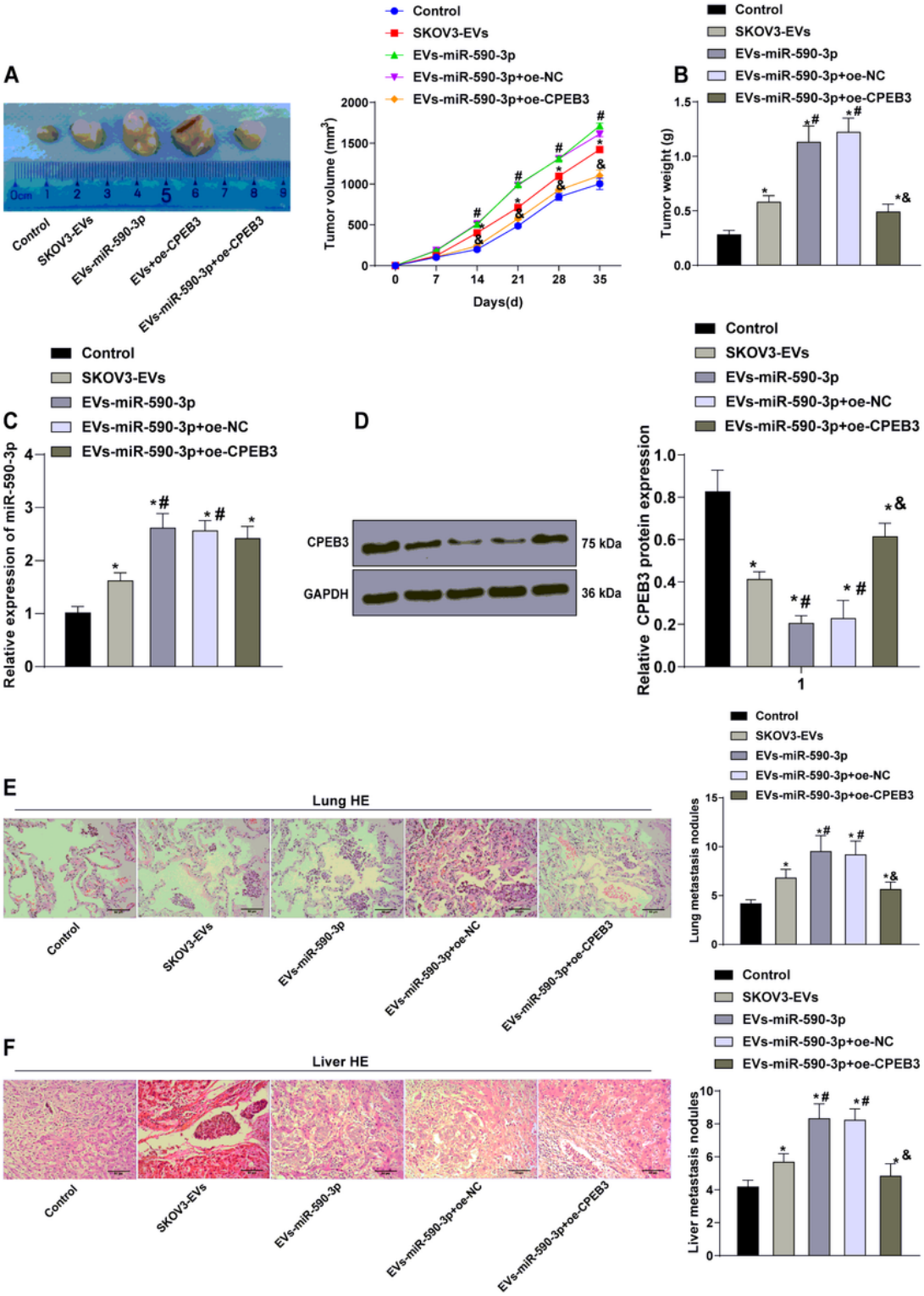

Figure 6

EVs-miR-590-3p facilitated tumorigenesis and metastasis in vivo by repressing CPEB3. A: SKOV3 cells were subcutaneously injected into nude mice; the tumor size was measured once a week and the growth curve was drawn; at the 5th week, the nude mice were euthanized and the tumor tissues were taken for photos. B: Tumor weight; C: miR-590-3p expression in tumor tissues was detected using RT-qPCR. D: Expressions of CPEB3, Lin28b and NRP-1 were detected using Western blotting. F: Lung metastasis model was established in nude mice, and lung tissues of nude mice was stained with HE after 30 days, scale bar = 50 μm. G: Liver metastasis model was established in nude mice, and liver tissues of nude mice was stained with HE after 30 days, scale bar = 50 μm. * vs. the control group, $p < 0.05$, # vs. the SKOV3-EVs group, $p < 0.05$, & vs. the EVs-miR-590-3p + oe-NC group, $p < 0.05$. Data are presented as mean ± standard deviation. One-way ANOVA was used to analyze the data among multiple groups, and repeated measurement ANOVA was used to compare the tumor volume at different time points. N = 8.

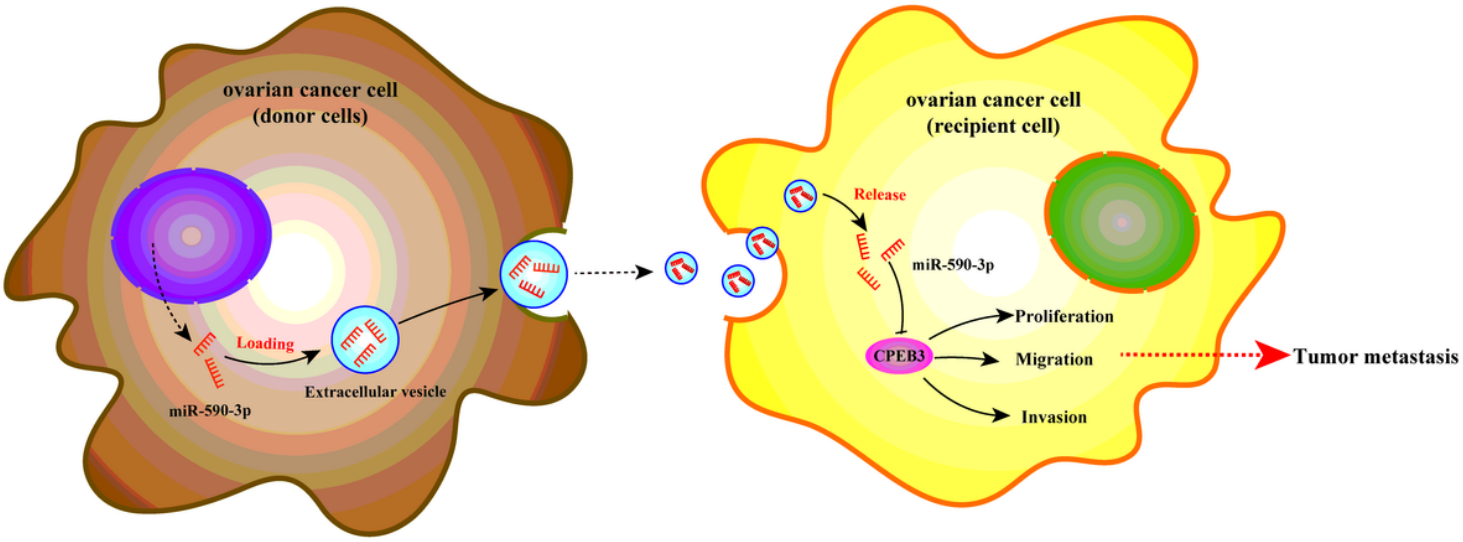

Figure 7

OC cell-derived EVs facilitated OC metastasis via the miR-590-3p/CPEB3 axis.